Developing a Head-Attached Interface Device for Closed-Loop Transcranial Ultrasound Stimulation in the Mouse Brain

Ryo Furukawa[1] [a], Shuichi Murakami[2] [b] and Takashi Tateno[3] [c]

[1]*Bioengineering and Bioinformatics, Graduate School of Information Science and Technology, Hokkaido University, Kita 14, Nishi 9, Kita-ku, Sapporo, Hokkaido 060-0814, Japan*
[2]*Osaka Research Institute of Industrial Science and Technology, 2-7-1, Ayumino, Izumi, Osaka, 594-1157, Japan*
[3]*Bioengineering and Bioinformatics, Faculty of Information Science and Technology, Hokkaido University, Kita 14, Nishi 9, Kita-ku, Sapporo, Hokkaido 060-0814, Japan*

Abstract: Transcranial ultrasound stimulation (TUS), which can be used to noninvasively stimulate local and deep brain areas, holds significant promise for clinical applications. However, TUS apparatus is typically constructed with several components, including a relatively large single-element ultrasound (US) transducer, a waveguide, and a driving source. These components pose challenges when conducting experiments with freely moving small animals, especially in the context of wearable devices. Additionally, conventional open-loop stimulation systems do not allow for the simultaneous monitoring of neural activity, which can sometimes result in the overactivation of neural responses. In this study, we developed a head-mounted piezoelectric micromachined ultrasound transducer (PMUT) array with integrated monitoring electrodes to serve as a TUS interface for mice. To determine effective array patterns for optimal US beam profiles, we first conducted beamforming simulations. We then microfabricated the PMUT arrays according to the results of these simulations. Subsequently, we performed electroencephalographic (EEG) recordings to evaluate the potential of TUS in mice while simultaneously monitoring neural activities. Finally, we discuss future applications of a closed-loop TUS system in the treatment of brain diseases.

1 INTRODUCTION

Neuromodulation has been utilized as a clinical tool for treating brain disorders (Davidson et al., 2024; Mattioli et al., 2024). However, conventional neuromodulation techniques, including electromagnetic stimulation, face challenges related to spatial resolution, invasiveness, and effective transmission to deep brain regions (Rezayat & Toostani, 2016).

Transcranial ultrasound stimulation holds promise for clinical applications owing to its low or non-invasive nature, high spatial resolution, and ability to transmit mechanical vibrations into the brain to induce neuromodulation (Tufail et al., 2010). Recently, miniaturized devices based on microelectromechanical system (MEMS) technology have been reported for the purpose of ultrasound (US) neuromodulation (Jo et al., 2019). However, because the conventional transcranial ultrasound stimulation (TUS) devices used in animals are specialized for brain stimulation itself, simultaneously monitoring neural activity driven by these devices requires separate recording systems from the stimulation devices (H. Kim et al., 2019; Zhou et al., 2019). Therefore, the integration of stimulation and recording devices is beneficial for realizing an *on-demand stimulation paradigm*, which would enable brain stimulation as needed for short periods without causing overstimulation. More specifically, deep brain stimulation (DBS) is utilized as one of the symptomatic treatments for Parkinson's disease and

[a] https://orcid.org/0000-0001-8920-1025
[b] https://orcid.org/0000-0002-8862-8446
[c] https://orcid.org/0000-0001-9429-9880

has demonstrated clinical efficacy in alleviating symptoms (Okun, 2012). Currently, DBS systems are commonly implemented using an open-loop configuration; however, this approach has associated with side effects, including the induction of neural hyperactivity. To address these challenges, a closed-loop DBS system that monitors neural activity and adaptively delivers stimulation as needed is being explored as a promising solution (Little et al., 2016).

Conventional TUS devices are open-loop stimulators, which can sometimes induce excessive neural activity, whereas the on-demand stimulation paradigm requires a closed-loop stimulation system (Takeuchi & Berényi, 2020). Although several studies have reported methods for closed-loop TUS systems (Jo et al., 2022; Xie et al., 2022), in these studies, the stimulator and monitoring electrodes were not packaged together as one device. For future applications for chronic conditions in small animal models such as rodents, small-sized systems using an integrated device are desired.

Here, we describe our development of a head-attached interface device for TUS applied to mice in a closed-loop manner. This paper primarily describes: (i) the design of a closed-loop TUS device, (ii) a fabrication method to realize this design, and (iii) a demonstration of the device's usefulness by analyzing electroencephalographic (EEG) data recorded from a mouse head through the incorporated monitoring electrodes. First, we describe the design of a piezoelectric micromachined ultrasound transducer (PMUT) combined with monitoring electrodes. Second, we explain our detailed microfabrication method. Third, we present EEG recordings to examine whether the head-attached device could be used for monitoring neural activities. Finally, we discuss future applications of a wearable closed-loop TUS system for the treatment of human brain diseases.

2 METHODS

2.1 Design

To achieve TUS in a mouse brain, we aimed to develop a PMUT with several diaphragms, the design and structure of which were based on a previous study (Furukawa et al., 2024). The PMUT is designed to meet the following three conditions: (i) a resonant frequency of 500 kHz for each diaphragm, (ii) ultrasound pressure generated by mechanical oscillations greater than 100 kPa, and (iii) a focal length of over 5 mm (Yuan et al., 2021). Additionally,

microelectrodes (200×200 μm) were designed on the back side of the PMUT to monitor EEG signals from a mouse. The size of the microelectrodes was determined on the basis of a previous report that demonstrated low electrode impedance with the same size and materials (Furukawa et al., 2024).

The structure of the PMUT is similar to that of a previously reported device (Furukawa et al., 2024), and consists of the following five components: (1) a lead zirconate titanate (PZT) plate, (2) a silicon (Si) layer, (3) an SiO_2 membrane, (4) top and bottom Pt/Ti electrodes, and (5) an Si supporting layer. To operate the diaphragm as a transducer and generate acoustic pressure, a thin film of piezoelectric material was used to convert electrical (voltage) signals into ultrasound pressure changes. To obtain a thin diaphragm that could function as a vibrating plate, circular openings were designed from the rear side of the supportive Si substrate.

Before fabricating the device, we numerically simulated the vibrations of diaphragms in the PMUT using general-purpose physics simulation software (COMSOL Multiphysics, Ver. 6.2, COMSOL AB, Sweden) on a supercomputer system (PRIMERGY CX400/CX2550, FUJITSU, Japan) at the Hokkaido University Computer Centre. Using the finite element method (FEM) in this simulation software, we calculated the primary resonant frequency, targeting 500 kHz, and determined the required sizes for the PMUT.

Next, to explore the effective design of a US array for TUS within a restricted area (10×10 mm), we conducted a beamforming simulation with two variable parameters with the aim of achieving target acoustic pressures and focal length: (i) the distance between the centers of diaphragms (d) ranging from 1 to 2 mm in 0.5-mm steps; and (ii) the excitation time delay (Δt) ranging from 0 to 1.8 μs in 0.2-μs steps (Fig. 1A) when used as a phased array system. The excitation time delay was used to steer the US beam. For this numerical simulation, the combinations of the distance d and the total number of diaphragms (cells) in individual PMUTs for our explored design are summarized in Table 1.

Table 1: Design of the PMUT phased array used in the beamforming simulation.

d (mm)	Total cell number
1.0	25
1.5	17
2.0	17

In our simulation, for the acoustic pressure p_t, the wave equation is described as:
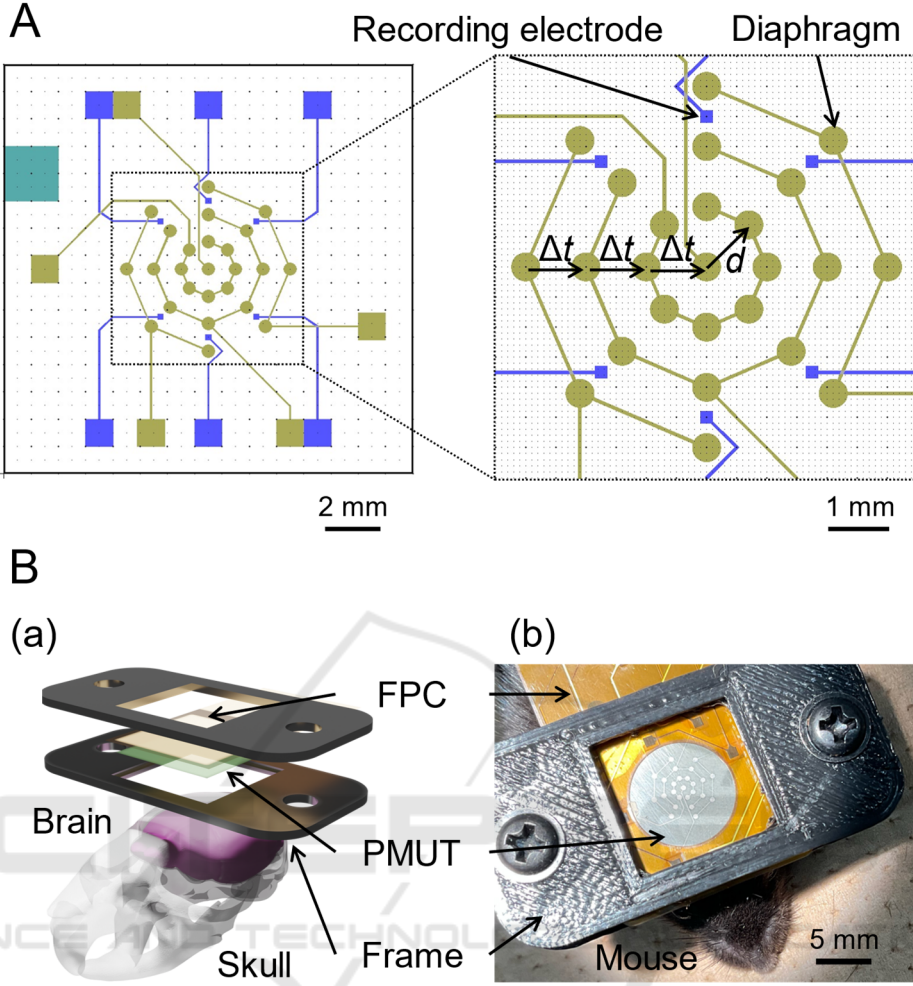
Figure 1: The design of a wearable PMUT phased array for closed-loop TUS. (A) Overall patterns of the PMUT design (left view) and an enlarged view of the centre part (right panel). Gold lines, squares, and circles represent the upper electrodes and their pads used to drive the transducer. Green squares are contact holes of the bottom electrode. Blue small and large squares are microelectrodes and their pads used to acquire EEG signals from mice. (B) (a) Schematic of the head-attached type PMUT. A surgically fixed bottom frame and removable top frame hold the PMUT. (b) Image of the fully packaged PMUT device.

$$\nabla \cdot \left\{ -\frac{1}{\rho}(\nabla p_t - \mathbf{q}_d) \right\} - \frac{k^2 p_t}{\rho} = Q_m, \tag{1}$$

$$k^2 = \left(\frac{2\pi f}{c}\right)^2 \tag{2}$$

where ρ is the density of the medium, c is the speed of sound, f is the driving US frequency, parameter $\mathbf{q}_d$ is the dipole domain source (which represents a domain volumetric force), and Q_m is the monopole domain source for a uniform strength in all directions.

Several PMUTs have recently been reported for neuromodulation in rodents. A 1D-array PMUT with a 275-μm radius for each diaphragm was reported, with a single transducer generating 67.3 kPa with an applied voltage of 66 V (Lee et al., 2019; Oh et al., 2019). A 2D-array PMUT with a 580-μm radius for each diaphragm was also reported, for which a single transducer generated 65.6 ± 1.8 kPa with an applied voltage of 70 V (Furukawa et al., 2024). In these previous reports, the acoustic pressures were all measured at a distance of approximately 1 mm away from the devices. Therefore, in the structural model of our simulation, we determined 60 kPa at 1 mm from each diaphragm to be the desired acoustic pressure value generated (i.e., 1.25 MPa).

2.2 Microfabrication and Packaging

Our microfabrication process was based on a previous report on the standard MEMS technology (Kuwano et al., 2020). The initial substrate was a silicon-on-insulator (SOI) wafer consisting of the following three layers: a device layer (Si, 15 μm), an insulating

membrane (SiO_2, 1 μm), and a handle layer (Si, 500 μm) with a 1-μm thermal-oxidized SiO_2 layer. Briefly, our microfabrication process was as follows:

1. To form the microelectrode, a layer consisting of a 100-nm-thick Pt coating and a 10-nm-thick Ti coating was deposited on the back side of the substrate using a sputtering system (RSC-3ERD, Riken-sha Co., Japan).

2. Subsequently, the recording electrodes and their wires were patterned on the back side by photolithography using an inductively coupled plasma reactive ion etching (ICP-RIE) system (RIE-101HU, SUMCO Co., Japan).

3. Next, the protective film (TMMR 2000SV, TOKYO OHKA KOGYO CO., LTD.) for the wires was formed on the bottom side.

4. A contact hole to expose the bottom electrode of the PMUT was formed on the front side of the substrate using a Deep-RIE instrument (MUC-21 ASE-SRE, SPP Technologies Co., Japan).

5. A PZT plate with a thickness of 100 μm (PI Japan) was attached to the front side of the SOI substrate with an epoxy adhesive (E205, Konishi Co., Ltd.).

6. The thickness of the PZT plate was reduced to 40 μm by using a griding machine (Mechatec300 SPC, Kitagawa GRESTECH Co., Ltd.).

7. In order to form the top electrodes of the PZT and their lead wires, a layer consisting of a 100-nm-thick Pt coating and a 10-nm-thick Ti coating was deposited using a sputtering system, and was patterned using a lift-off technique.

8. To create the diaphragm shape, the Si handle layer was removed from the back side using a Deep-RIE instrument (MUC-21 ASE-SRE, SPP Technologies Co., Japan).

After the process, the fabricated PMUT device was packaged with the flexible printed circuit board (Fig. 1B).

2.3 Measuring Event-Related Potentials

2.3.1 Surgical Procedure

In this study, all animal experiments were carried out in accordance with the NIH Guide for the Care and Use of Laboratory Animals and with approval from the International Animal Care and Use Committee of Hokkaido University. For the animal experiments, two female and one male C57BL/6J mice (Japan SLC, Japan; 7 to 8 weeks old) were used. Intraperitoneal injections of a mixture of medetomidine (0.3 mg/kg), midazolam (4.0 mg/kg), and butorphanol (5.0 mg/kg) were used to initiate anesthesia, and anesthesia levels were confirmed by the level of response when pinching the leg (Yoshikawa et al., 2023).

The fur on top of the skull was gently removed, then the scalp was carefully excised to expose the skull. The custom-made 3D-printed bottom frame (20 × 40 mm; the center was positioned at the lambda) was attached to hold the packaged PMUT by sandwiching it with the top frame (Fig. 1B). The gap between the PMUT and skull was filled with US gel.

2.3.2 Signal Recording and Sound Stimuli

The sensing microelectrodes were examined to detect neural activities in extracellular field potentials through EEG recordings. Pure-tone burst sounds (frequencies: 2, 4, 8, 16, and 32 kHz; sound intensity: 80 dB sound pressure level [SPL]; duration: 100 ms) were used to record the sound event-related potentials (ERPs) in response to the acoustic stimulation. We used linearly increasing onset and decreasing offset stimulus envelopes set at 10% of the total duration of each stimulus. Sound stimuli were presented via a speaker (MF1; Tucker-Davis Technologies). The EEG signals were recorded at a sampling rate of 1 kHz. Fifty trials were conducted under the same conditions.

2.4 Data Analysis

All statistical analyses were performed using order statistics without assuming a specific distribution, employing non-parametric statistical methods. EEG data were compared using the Wilcoxon signed-rank test with Python (Ver. 3.12.1). The statistical analyses were conducted for data acquired at two channels (Chs 4 and 6) located at the inferior colliculus (IC). We defined the baseline amplitude as the averaged pre-stimulus peak amplitude before the stimulation onset. In contrast, an ERP amplitude for 0.5 s after the onset of a stimulus was defined as the post-stimulus peak amplitude.
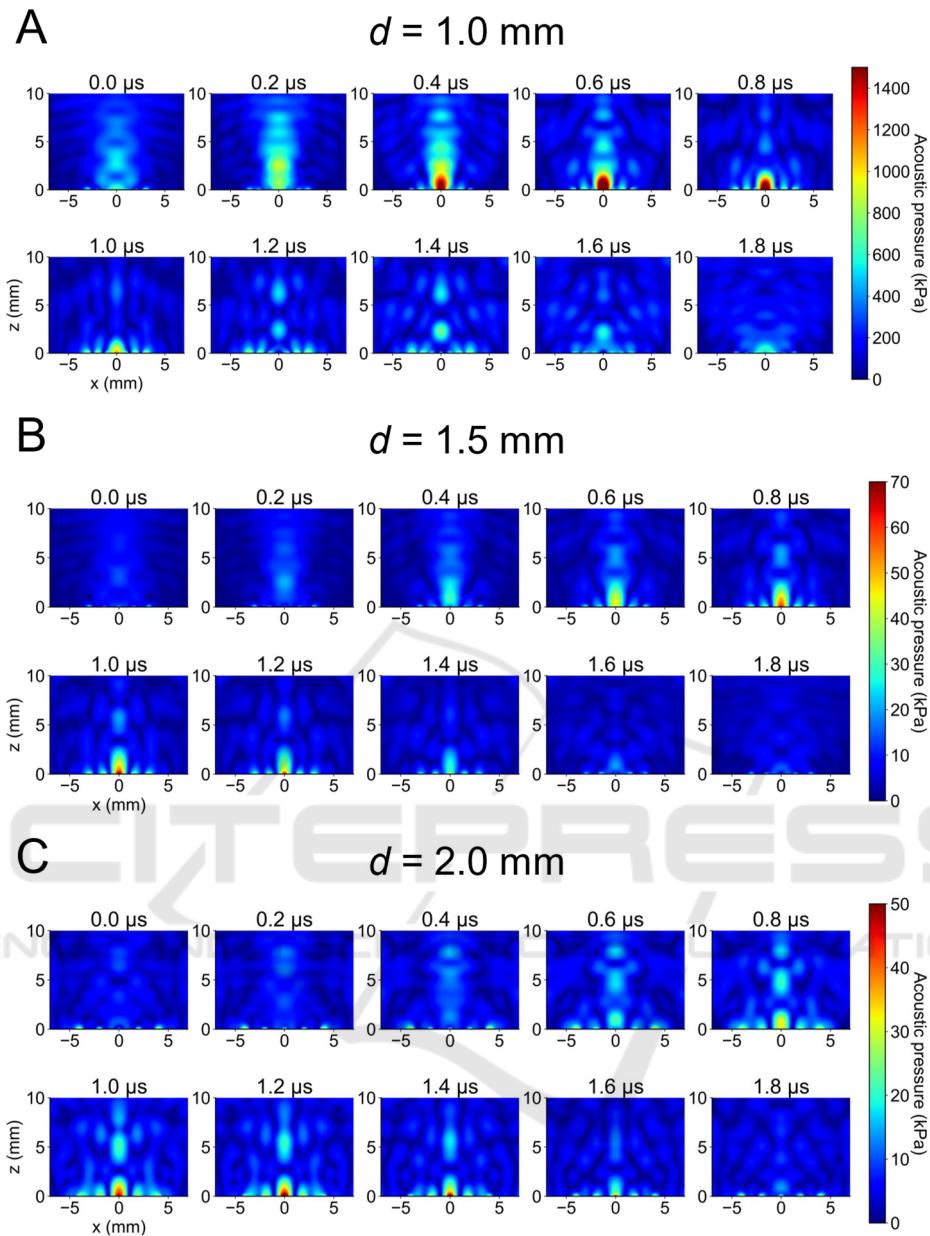
Figure 2: Simulated US beam profiles of the PMUT phased array. The distance (*d*) is represented in the right panel of Fig. 1A.

3 RESULTS

3.1 Ultrasound Beamforming

On the basis of the results of the numerical calculations for our PMUT structural model with a resonant frequency of 500 kHz, we selected the following size parameters: a diaphragm radius of 235 μm, a PZT layer thickness of 40 μm, and a Si layer thickness of 15 μm. Subsequently, using these determined diaphragm sizes, we conducted a beamforming simulation of the designed PMUT (Fig. 1A), in which each diaphragm array had different nearest distances (*d*) between diaphragms (*d* = 1.0, 1.5, and 2.0 mm) and/or different total numbers of diaphragms (17 or 25 cells, see Table 1). For example, for the array pattern of *d* = 1.0 mm and 27 diaphragms, Fig. 2A illustrates the two-dimensional (2D; *x-z* field) acoustic pressure distributions at *y* = 0 mm in the 3D acoustic field, resulting in a far-field peak at over 5 mm with a peak pressure exceeding hundreds of kPa. Moreover, with the array pattern of *d* = 1.5 mm (or
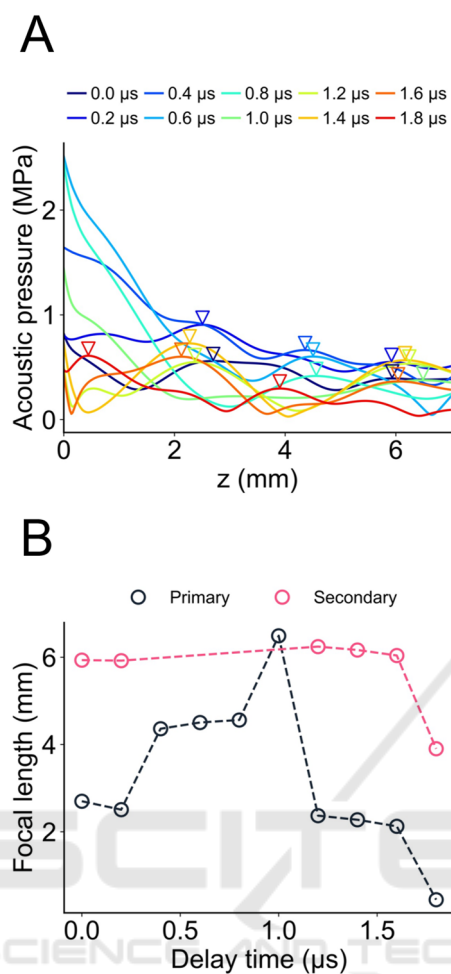
A

B

Figure 3: US beam profile for the axial distance in Fig. 2. (A) Acoustic pressure distribution with different delay times in the array pattern of $d = 1.0$ mm (Fig. 2A). Each inverted triangle marker represents a local peak under the delay time. (B) Focal length and delay times for primary and secondary peaks indicated in panel (A). For some delay time conditions, no secondary peaks were detected.

2.0 mm) and 17 diaphragms, although a far-field peak exists at approximately 5 mm in the 2D field with the axial direction (perpendicular to the PMUT array surface), the simulated acoustic pressures were smaller (in the tens of kPa) compared with the array pattern of $d = 1.0$ mm (Figs. 2B, C). The acoustic field in the axial direction (i.e., z direction) for the array pattern of $d = 1.0$ mm is shown in Fig. 3A. The inverted triangle markers represent the primary or secondary peaks (local maxima). The focal lengths depending on the delay times (Δt) of the phased array are summarized in Fig. 3B. We found that using a delay time Δt of 1.0 μs, a primary peak in the acoustic field showed a local maximum at the farthest-most field. This result suggests that using the delay time

(e.g., $\Delta t = 0.6$ μs for the surface or $\Delta t = 1.4$ μs for the center) and a 70-V input voltage to the PMUT, the US beam generated by the array of $d = 1.0$ mm can reach a brain target within a range from the surface to the center of a mouse brain.

3.2 Packaging of the Wearable PMUT

We successfully microfabricated the PMUT phased array and integrated it with a custom-made flexible printed circuit (FPC). The total weight of the packaged device, including the head frames, PMUT, FPC, and any other components, was 1.40 g.

3.3 Event-Related Potentials

To examine the device's ability to detect neural activity from EEG signals, we conducted ERP recordings in response to sound stimulation. The schematic for the EEG recordings with six monitoring electrodes (Chs 1 to 6) is illustrated in Fig. 4A. Additionally, a typical example of averaged waveforms evoked by sound stimuli (4-kHz pure-tone burst, 80 dB SPL) is shown in Fig. 4B. The waveforms obtained from two channels (e.g., Chs 4 and 6 in Fig. 4B) located around the IC showed negative and positive peaks after sound stimulation onset (−4.9 μV and 6.6 μV at Ch 4 in Fig. 4B). Furthermore, averaged waveforms obtained from Ch 4 in response to sound stimulation with different frequencies are illustrated in Fig. 4Ca. Negative or positive peaks after the onset of the stimulation were observed in response to the pure-tone bursts examined (Fig. 4Ca). In particular, ERP peaks (post-amplitudes) larger than the corresponding baseline amplitudes (pre-amplitudes) were detected in response to 4- and 8-kHz pure-tone burst stimuli (*$p < 0.05$, $n = 6$ from three animals). In contrast, no significant differences were found between pre and post peak amplitudes in responses to the stimuli with 2, 16, and 32 kHz.

4 DISCUSSION

The total weights of previously reported wearable transducers for rodents were 0.765 and 20 g for rats (E. Kim et al., 2021; H. Kim et al., 2019), and 2 g for mice (Zhou et al., 2019). Since our developed device has a total weight of 1.4 g, we suggest that it is suitable for application in experiments with freely moving mice. However, the signal generator and driving voltage source are not included in our weight measurement.

In this study, we describe the development of a MEMS-based PMUT phased array as a wearable TUS interface device for closed-loop stimulation. The resonant frequency of a single element transducer was first calculated, followed by determination of the sizes and the structure. Subsequently, US beamforming was simulated with 25 or 17 cells with a variable delay time for the driving signals of the phased array. Guided by the numerical findings, we proceeded to design and microfabricate wearable PMUTs featuring 25 circular diaphragms, and incorporating six square monitoring electrodes. To our knowledge, this is the first report of the packaging of monitoring electrodes onto a wearable PMUT. With regard to the results of the beamforming

simulation, we expect to be able to modulate neural activity with the output US beam. In addition, we suggest that the focal length can be manipulated across a wide range of regions in the mouse brain by adjusting the excitation delay time (Figs. 3A, B). To experimentally confirm the simulated beam profiles, we will measure the acoustic pressure distribution with a needle hydrophone (Furukawa et al., 2022).

Next, we demonstrated sound-driven EEG recordings as a step towards the future application of a wearable closed-loop TUS system. We successfully detected the sound ERPs with the incorporated electrodes, and since the IC is located 2–3 mm caudal to the lambda and 2 mm lateral to the midline, the observed ERPs could possibly be attributed to
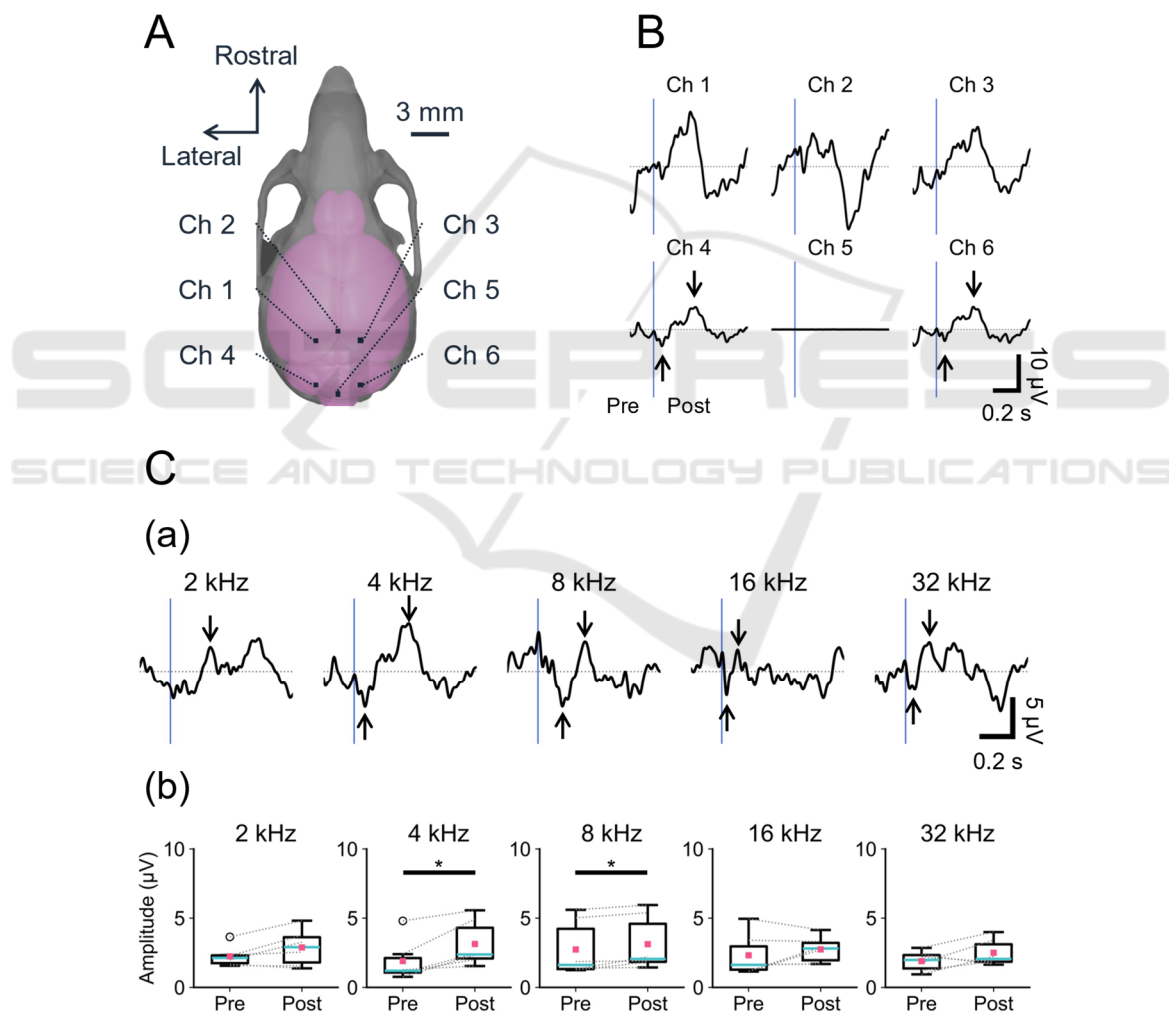

Figure 4: Sound ERP waveforms at six sites on the mouse skull. (A) The six recording sites on the mouse skull are illustrated with channel numbers (Chs 1 to 6). (B) Averaged ERP waveforms in response to sound stimulation (pure-tone burst, 4 kHz, 80 dB SPL). (C) ERP waveforms recorded at (a) Ch 4 and (b) comparison between pre- and post-maximum amplitudes of the pure-tone burst with different frequencies (*$p < 0.05$, $n = 6$ from three animals). The timings of the sound onset are represented by vertical blue bars.

neural activity in the IC. Lower frequencies (e.g., 4 kHz) tend to evoke neural activity in shallow laminae in the mouse IC (Sato et al., 2024), which is consistent with the frequency characteristic of our observed ERPs (Figs. 4Ca, 4b).

In future applications, we plan to test this device in closed-loop TUS as a treatment method for brain diseases. In line with this purpose, the oscillatory power of specific frequencies is utilized as a reliable EEG biomarker. Further, EEG biomarkers play a pivotal role in diagnosing and understanding neurological disorders, including epilepsy (Buchhalter et al., 2022; Saeedinia et al., 2024), Alzheimer's disease (Chetty et al., 2024; Meghdadi et al., 2021), and psychiatric disorders (Abi-Dargham & Horga, 2016). In future applications of our device, EEG biomarkers could provide PMUT device uses with invaluable data for early detection and intervention by capturing aberrations in brain activity characteristics.

ACKNOWLEDGEMENTS

REFERENCES

Abi-Dargham, A., & Horga, G. (2016). The search for imaging biomarkers in psychiatric disorders. *Nature Medicine*, *22*(11), 1248–1255. https://doi.org/10. 1038/nm.4190

Buchhalter, J., Neuray, C., Cheng, J. Y., D'Cruz, O., Datta, A. N., Dlugos, D., French, J., Haubenberger, D., Hulihan, J., Klein, P., Komorowski, R. W., Kramer, L., Lothe, A., Nabbout, R., Perucca, E., & der Ark, P. V. (2022). EEG parameters as endpoints in epilepsy clinical trials—An expert panel opinion paper. *Epilepsy Research*, *187*, 107028. https://doi.org/10. 1016/j.eplepsyres.2022.107028

Chetty, C. A., Bhardwaj, H., Kumar, G. P., Devanand, T., Sekhar, C. S. A., Aktürk, T., Kiyi, I., Yener, G., Güntekin, B., Joseph, J., & Adaikkan, C. (2024). EEG biomarkers in Alzheimer's and prodromal Alzheimer's: A comprehensive analysis of spectral and connectivity features. *Alzheimer's Research & Therapy*, *16*(1), 236. https://doi.org/10.1186/s13195-024-01582-w

Davidson, B., Bhattacharya, A., Sarica, C., Darmani, G., Raies, N., Chen, R., & Lozano, A. M. (2024). Neuromodulation techniques – From non-invasive brain stimulation to deep brain stimulation. *Neurotherapeutics*, *21*(3), e00330. https://doi. org/10.1016/j.neurot.2024.e00330

Furukawa, R., Kaneta, H., & Tateno, T. (2022). A Multielectrode Array-Based Recording System for Analyzing Ultrasound-Driven Neural Responses in Brain Slices in vitro. *Frontiers in Neuroscience*, *16*. https://www.frontiersin.org/articles/10.3389/fnins.202 2.824142

Furukawa, R., Yoshikawa, T., Murakami, S., & Tateno, T. (2024). A piezoelectric micromachined ultrasound transducer combined with recording electrodes for acute brain preparations in vitro. *Journal of Neuroscience Methods*, *403*, 110048. https://doi.org/10.1016/j.jneumeth.2023.110048

Jo, Y., Lee, S.-M., Jung, T., Park, G., Lee, C., Im, G. H., Lee, S., Park, J. S., Oh, C., Kook, G., Kim, H., Kim, S., Lee, B. C., Suh, G. S. B., Kim, S.-G., Kim, J., & Lee, H. J. (2022). General-Purpose Ultrasound Neuromodulation System for Chronic, Closed-Loop Preclinical Studies in Freely Behaving Rodents. *Advanced Science*, *9*(34), 2202345. https://doi.org/10. 1002/advs.202202345

Jo, Y., Oh, C., & Lee, H. J. (2019). Microelectromechanical Systems-Based Neurotools for Non-Invasive Ultrasound Brain Stimulation. *Chronobiology in Medicine*, *1*(2), 55–59. https://doi.org/10. 33069/cim.2019.0009

Kim, E., Anguluan, E., Kum, J., Sanchez-Casanova, J., Park, T. Y., Kim, J. G., & Kim, H. (2021). Wearable transcranial ultrasound system for remote stimulation of freely moving animal. *IEEE Transactions on Biomedical Engineering*, *68*(7), 2195–2202. https://doi.org/10.1109/TBME.2020.3038018

Kim, H., Kim, S., Sim, N. S., Pasquinelli, C., Thielscher, A., Lee, J. H., & Lee, H. J. (2019). Miniature ultrasound ring array transducers for transcranial ultrasound neuromodulation of freely-moving small animals. *Brain Stimulation*, *12*(2), 251–255. https://doi.org/10. 1016/j.brs.2018.11.007

Kuwano, T., Kaneta, H., Nishikawa, J., Satoh, K., Murakami, S., & Tateno, T. (2020). Developing a Frequency-selective Piezoelectric Acoustic Sensor Sensitive to the Audible Frequency Range of Rodents. *IEEJ Transactions on Electrical and Electronic Engineering*, *15*(12), 1816–1823. https://doi.org/10. 1002/tee.23260

Lee, J., Ko, K., Shin, H., Oh, S.-J., Lee, C. J., Chou, N., Choi, N., Tack Oh, M., Chul Lee, B., Chan Jun, S., & Cho, I.-J. (2019). A MEMS ultrasound stimulation system for modulation of neural circuits with high spatial resolution in vitro. *Microsystems & Nanoengineering*, *5*(1), Article 1. https://doi.org/10. 1038/s41378-019-0070-5

Little, S., Tripoliti, E., Beudel, M., Pogosyan, A., Cagnan, H., Herz, D., Bestmann, S., Aziz, T., Cheeran, B., Zrinzo, L., Hariz, M., Hyam, J., Limousin, P., Foltynie, T., & Brown, P. (2016). Adaptive deep brain stimulation for Parkinson's disease demonstrates reduced speech side effects compared to conventional stimulation in the acute setting. *Journal of Neurology, Neurosurgery & Psychiatry*, *87*(12), 1388–1389. https://doi.org/10.1136/jnnp-2016-313518

Mattioli, F., Maglianella, V., D'Antonio, S., Trimarco, E., & Caligiore, D. (2024). Non-invasive brain stimulation for patients and healthy subjects: Current challenges and future perspectives. *Journal of the Neurological Sciences*, *456*, 122825. https://doi.org/10.1016/j.jns.2023.122825

Meghdadi, A. H., Karić, M. S., McConnell, M., Rupp, G., Richard, C., Hamilton, J., Salat, D., & Berka, C. (2021). Resting state EEG biomarkers of cognitive decline associated with Alzheimer's disease and mild cognitive impairment. *PLOS ONE*, *16*(2), e0244180. https://doi.org/10.1371/journal.pone.0244180

Oh, S.-J., Lee, J. M., Kim, H.-B., Lee, J., Han, S., Bae, J. Y., Hong, G.-S., Koh, W., Kwon, J., Hwang, E.-S., Woo, D. H., Youn, I., Cho, I.-J., Bae, Y. C., Lee, S., Shim, J. W., Park, J.-H., & Lee, C. J. (2019). Ultrasonic Neuromodulation via Astrocytic TRPA1. *Current Biology*, *29*(20), 3386-3401.e8. https://doi.org/10.1016/j.cub.2019.08.021

Okun, M. S. (2012). Deep-Brain Stimulation for Parkinson's Disease. *New England Journal of Medicine*, *367*(16), 1529–1538. https://doi.org/10.1056/NEJMct1208070

Rezayat, E., & Toostani, I. G. (2016). A review on brain stimulation using low intensity focused ultrasound. *Basic and Clinical Neuroscience*, *7*(3), 187–194. https://doi.org/10.15412/J.BCN.03070303

Saeedinia, S. A., Jahed-Motlagh, M. R., Tafakhori, A., & Kasabov, N. K. (2024). Diagnostic biomarker discovery from brain EEG data using LSTM, reservoir-SNN, and NeuCube methods in a pilot study comparing epilepsy and migraine. *Scientific Reports*, *14*(1), 10667. https://doi.org/10.1038/s41598-024-60996-6

Sato, H., Sugimoto, F., Furukawa, R., & Tateno, T. (2024). Modulatory Effects on Laminar Neural Activity Induced by Near-Infrared Light Stimulation with a Continuous Waveform to the Mouse Inferior Colliculus In Vivo. *eNeuro*, *11*(5). https://doi.org/10.1523/ENEURO.0521-23.2024

Takeuchi, Y., & Berényi, A. (2020). Oscillotherapeutics – Time-targeted interventions in epilepsy and beyond. *Neuroscience Research*, *152*, 87–107. https://doi.org/10.1016/j.neures.2020.01.002

Tufail, Y., Matyushov, A., Baldwin, N., Tauchmann, M. L., Georges, J., Yoshihiro, A., Tillery, S. I. H., & Tyler, W. J. (2010). Transcranial Pulsed Ultrasound Stimulates Intact Brain Circuits. *Neuron*, *66*(5), 681–694. https://doi.org/10.1016/j.neuron.2010.05.008

Xie, Z., Yan, J., Dong, S., Ji, H., & Yuan, Y. (2022). Phase-locked closed-loop ultrasound stimulation modulates theta and gamma rhythms in the mouse hippocampus.

Frontiers in Neuroscience, *16*. https://www.frontiersin.org/articles/10.3389/fnins.2022.994570

Yoshikawa, T., Sato, H., Kawakatsu, K., & Tateno, T. (2023). Low-Cost Electroencephalographic Recording System Combined with a Millimeter-Sized Coil to Transcranially Stimulate the Mouse Brain In Vivo. *JoVE (Journal of Visualized Experiments)*, *195*, e65302. https://doi.org/10.3791/65302

Yuan, Y., Zhang, K., Zhang, Y., Yan, J., Wang, Z., Wang, X., Liu, M., & Li, X. (2021). The Effect of Low-Intensity Transcranial Ultrasound Stimulation on Neural Oscillation and Hemodynamics in the Mouse Visual Cortex Depends on Anesthesia Level and Ultrasound Intensity. *IEEE Transactions on Biomedical Engineering*, *68*(5), 1619–1626. IEEE Transactions on Biomedical Engineering. https://doi.org/10.1109/TBME.2021.3050797

Zhou, H., Niu, L., Xia, X., Lin, Z., Liu, X., Su, M., Guo, R., Meng, L., & Zheng, H. (2019). Wearable Ultrasound Improves Motor Function in an MPTP Mouse Model of Parkinson's Disease. *IEEE Transactions on Biomedical Engineering*, *66*(11), 3006–3013. IEEE Transactions on Biomedical Engineering. https://doi.org/10.1109/TBME.2019.2899631.